Mössbauer and Magnetization Studies of Heme−Copper-Bridged Assemblies Pertinent to Cytochrome *c* Oxidase

Karl E. Kauffmann,*[,1a] Christine A. Goddard,[1b] Yan Zang,[1c] R. H. Holm,[1b] and Eckard Münck*[,1a]

Departments of Chemistry, Carnegie Mellon University, Pittsburgh, Pennsylvania 15213, Harvard University, Cambridge, Massachusetts 02138, and the University of Minnesota, Minneapolis, Minnesota 55455

Received July 12, 1996[⊗]

In order to elucidate the structural and electronic properties of the dioxygen-reducing site of cytochrome oxidases, we have studied heme-based molecular assemblies containing the bridge unit $Fe^{III}-X-Cu^{II}$ with $X = O^{2-}$, OH^-, and HCO_2^-. Here we describe the results of Mössbauer and magnetization studies of $[(OEP)Fe-O-Cu(Me_6\text{-tren})]^{1+}$ (**3**), $[(OEP)Fe-(OH)-Cu(Me_5dien)(OClO_3)]^{1+}$ (**4**), $[(OEP)Fe-(O_2CH)-Cu(Me_5dien)(OClO_3)]^{1+}$ (**5**), and $[(OEP)Fe\{(O_2CH)Cu(Me_6tren)\}_2]^{3+}$ (**6**). On the basis of magnetization studies, the oxidized binuclear enzyme site has been reported to be strongly coupled, with an $S = 2$ ground state. For **3** and **4** the Mössbauer data were analyzed for strong antiferromagnetic coupling between a high-spin Fe(III) ($S_1 = {}^5/_2$) and Cu(II) ($S_2 = {}^1/_2$), resulting in an $S = 2$ ground state. The exchange coupling of hydroxo-bridged **4** is substantial, $J = 170$ cm^{-1} ($H_{ex} = J\mathbf{S}_1\cdot\mathbf{S}_2$), but is smaller than $J \geq 200$ cm^{-1} reported for oxo-bridged **3**. The collective evidence for synthetic complexes and the oxidized enzymes indicates that the $Fe^{III}-(OH)-Cu^{II}$ bridge unit is probable for the latter in the resting state. The similarity of properties of formate-inhibited and "slow" cytochrome oxidase has suggested a carboxylate bridge in the binuclear site. Formate-bridged **5** maintains an *anti*−*anti* carboxylate bridge conformation and has $J = +18$ cm^{-1}. While the bridge conformation of **5** might not apply to a putative carboxylate bridge in the binuclear enzyme site, the order-of-magnitude difference between the J values of **3**, **4**, and **5** suggests that no stereochemically possible μ-η^1:η^1 carboxylate bridge conformation is likely to approach the strong coupling ($J \geq 200$ cm^{-1}) of the formate-inhibited and "slow" enzyme forms. If carboxylate does bridge, the $\mu-\eta^2$ mode appears more likely. Complex **6**, which is not biologically pertinent, displays weak *ferromagnetic* coupling between a central high-spin Fe(III) and two Cu(II) sites, -0.50 cm$^{-1} < J < -0.10$ cm^{-1}.

Introduction

Enzymes belonging to the superfamily of heme−copper oxidases[2] contain the unique binuclear site heme a_3-Cu_B, which simultaneously catalyzes the reaction $O_2 + 4H^+ + 4e^- \rightarrow 2H_2O$ and promotes the translocation of protons. In the oxidized state, the site contains a tris(imidazole)-ligated Cu(II) atom and a high-spin Fe(III) heme which, in bovine heart cytochrome *c* oxidase (CcO), have been shown by magnetization studies to be magnetically coupled to afford an $S = 2$ ground state.[3,4] Crystallography of the bovine heart[5] and *Paracoccus denitrificans*[6] enzymes reveal copper−iron distances of 5.2 and 4.5 Å, respectively. The bridging atoms or groups which modulate the exchange coupling are not evident in the crystal structures.

Two kinetically distinct forms of oxidized bovine heart CcO have been identified and designated as "fast" or "slow" on the basis of their relative rates of binding exogenous cyanide.[7] The slow form differs from the fast form in that it establishes an integer-spin $g = 12$ EPR signal and a blue-shifted Soret band. Furthermore, the two forms can be distinguished by their saturation magnetization behavior.[4] Magnetic data were analyzed under the assumptions of both strong ($J > 100$ cm^{-1}) and weak ($J < 4$ cm^{-1}) antiferromagnetic coupling between the $S_1 = {}^5/_2$ and $S_2 = {}^1/_2$ sites. It was proposed, however, that the data were more readily described by assuming a strong coupling model. This yielded a ground-state $S = 2$ manifold having zero-field splittings of $D = +13$ cm^{-1} ($E/D = 0.23$) and -7 cm^{-1} ($E/D = 0.27$) for the fast and slow forms, respectively. Although the bridge which propagates the exchange interaction has not been identified, EXAFS results have suggested a chlorine or sulfur bridge with accompanying Fe−Cu distances of 3.70 Å in the *Bacillus subtilis* oxidase[8] and 3.96 Å in the bovine heart enzyme.[9] A reinvestigation of the *B. subtilis* enzyme by both Cu EXAFS and ENDOR detected the presence of an O/N Cu(II) ligand with an exchangeable proton.[10] This result is highly suggestive of a $Fe^{III}-(OH)-$

⊗ Abstract published in *Advance ACS Abstracts,* February 1, 1997.

(1) (a) Carnegie Mellon University. (b) Harvard University. (c) University of Minnesota.
(2) (a) Chan, S. I.; Li, P. M. *Biochemistry* **1990**, *29*, 1. (b) Babcock, G. T.; Wikström, M. *Nature* **1992**, *356*, 301. (c) Malmström, B. G. *Chem. Rev.* **1990**, *90*, 1247; *Acc. Chem. Res.* **1993**, *26*, 332. (d) Calhoun, M. W.; Thomas, J. W.; Gennis, R. B. *Trends Biochem. Sci.* **1994**, 19. (e) García-Horsman, J. A.; Barquera, B.; Rumbley, J.; Ma, J.; Gennis, R. B. *J. Bacteriol.* **1994**, *176*, 5587. (f) Einarsdóttir, O. *Biochim. Biophys. Acta* **1995**, *1229*, 129.
(3) Tweedle, M. F.; Wilson, L. J.; Garcia-Iniguez, L.; Babcock, G. T.; Palmer, G. *J. Biol. Chem.* **1978**, *253*, 8065.
(4) Day, E. P.; Peterson, J.; Sendova, M. S.; Schoonover, J.; Palmer, G. *Biochemistry* **1993**, *32*, 7855.
(5) Tsukihara, T.; Aoyama, H.; Yamashita, E.; Tomizaki, T.; Yamaguchi, H.; Shinzawa-Itoh, K.; Nakashima, R.; Yaono, R.; Yoshikawa, S. *Science* **1995**, *269*, 1069; **1996**, *272*, 1136.
(6) Iwata, S.; Ostermeier, C.; Ludwig, B.; Michel, H. *Nature* **1995**, *376*, 660.
(7) (a) Baker, G. M.; Noguchi, M.; Palmer, G. *J. Biol. Chem.* **1987**, *262*, 595. (b) Papadopoulos, P. G.; Walter, S. A.; Li, J.; Baker, G. M. *Biochemistry* **1991**, *30*, 840. (c) Weng, L.; Baker, G. M. *Biochemistry* **1991**, *30*, 5727.
(8) Powers, L.; Lauraeus, M.; Reddy, K. S.; Chance, B.; Wikström, M. *Biochim. Biophys. Acta* **1994**, *1183*, 504.
(9) Henkel, G.; Müller, A.; Weissgräber, S.; Buse, G.; Soulimane, T.; Steffens, G. C. M.; Nolting, H.-F. *Angew. Chem., Int. Ed. Engl.* **1995**, *34*, 1488.

S0020-1669(96)00826-9 CCC: $14.00

Cu^{II} group. Such a bridge might convert to $Fe^{III}-O-Cu^{II}$ at higher pH.

Fast-to-slow conversion of CcO is accomplished by incubation of the enzyme at low pH[7a] or at higher pH in the presence of formate.[11] Because the properties of the slow and formate-bound forms are very similar,[7,11−14] it has been suggested that endogenous carboxylate might be a bridging ligand in the binuclear site of the slow form[13b,14,15] and that formate might insert itself in a bridging position in its reaction with the fast form.[14] Displacement of the carboxylate bridge would then lead to a slower reaction with cyanide, which binds to heme a_3 and very likely acts as a bridging ligand.[16] Magnetic results for formate-bound CcO are reported to be consistent with an $S = 2$ ground state; $J \geq 400$ cm^{-1} was estimated from the susceptibility data.[12]

Because of the foregoing observations, we regard the heme-based bridge units $Fe^{III}-X-Cu^{II}$ with $X = O^{2-}$, OH^-, HCO_2^-, and CN^- to be of fundamental significance in interpreting and predicting the geometrical and electronic structures of the binuclear site of CcO and related oxidases. Consequently, we have prepared and structurally characterized a number of molecular heme-based bridged assemblies[16−19] as potential analogues of the binuclear site in different bridging arrangements. Complexes of primary interest in the present investigation are **1**−**6**, whose structures are schematically depicted in Figure 1.

$[Fe(OEP)(O_2CH)]$ (**1**)[17]

$[Cu(Me_5dien)(O_2CH)(MeOH)]^+$ (**2**)[17]

$[(OEP)Fe(\mu\text{-}O)Cu(Me_6tren)]^+$ (**3**)[18]

$[(OEP)Fe(\mu\text{-}OH)Cu(Me_5dien)(OClO_3)]^+$ (**4**)[19]

$[(OEP)Fe(\mu\text{-}O_2CH)Cu(Me_5dien)(OClO_3)]^+$ (**5**)[17]

$[(OEP)Fe\{(\mu\text{-}O_2CH)Cu(Me_6tren)\}_2]^{3+}$ (**6**)[17]

$[(F_8\text{-}TPP)Fe-O-Cu(tmpa)]^+$ (**7**)[20,21]

$[(F_8\text{-}TPP)Fe-(OH)-Cu(tmpa)]^{2+}$ (**8**)[21]

Complexes **1** and **2** serve as mononuclear versions of the Fe(III) and Cu(II) fragments covalently linked in the bridged assemblies and are useful for interpreting electronic and structural features. The high-spin stereochemistry of **1**, with the Fe(III) atom *ca.* 0.4−0.5 Å above the porphyrin mean plane, is maintained in **3**−**5**. Similarly, the distorted-square-pyramidal stereochemistry of **2** is maintained in **4** and **5**; the Cu(II) stereochemistry in **3** and **6** is trigonal bipyramidal, as in mononuclear $[Cu(Me_6tren)(O_2CH)]^+$.[17] The bridge in three different crystal forms of **3** is essentially linear (175−178°),[18] whereas that of **4** is substantially bent (Fe−O−Cu = 157°).[19] In **5**, the bridge conformation is *anti*−*anti*. In trinuclear centrosymmetric **6**, there are *two* formate bridges, each with the *syn*−*anti* conformation, and the Fe(III) atom is in the porphyrin plane. Related μ-oxo[20,21] (**7**) and μ-hydroxo[21] (**8**) complexes have been prepared by Karlin and co-workers;[20,21] their bridge structural parameters determined by crystallography (**7**) or EXAFS (**8**) are in good agreement with those of **3** and **4**. Note that the Fe−Cu distances in **3** and **4**, 3.57 and 3.80 Å, respectively,[18] are comparable to the Fe−Cu distances deduced from EXAFS analyses of the *Bacillus subtilis* oxidase[8] and the bovine heart[9] enzymes but are much shorter than in the enzyme X-ray structures.[5,6] This discrepancy between the EXAFS distances obtained from frozen solutions of enzyme and the X-ray-structure Fe−Cu distances obtained from enzyme crystals suggests the absence of the corresponding bridges in the crystals.

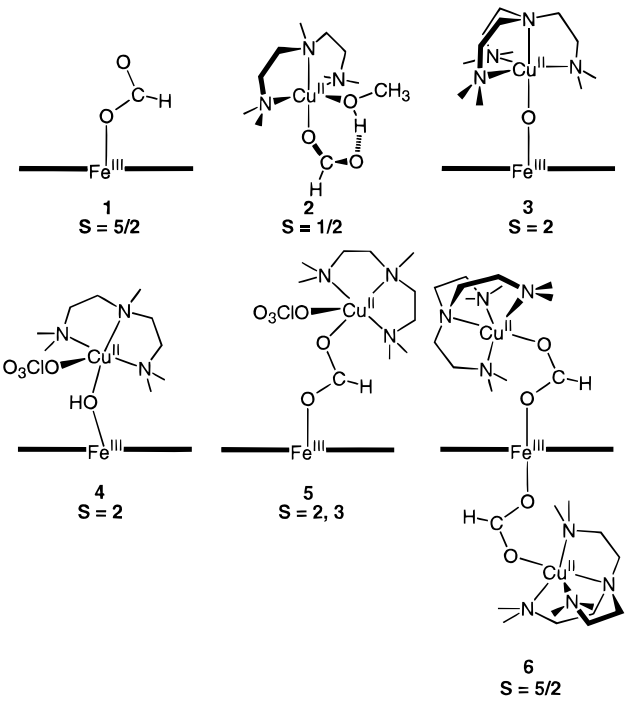

Figure 1. Schematic structures of mononuclear complexes **1** and **2** and bridged assemblies **3**−**6**, including selected structural parameters and ground-state spins. The horizontal line represents the porphyrin ligand; in **1** and **3**−**5** the Fe(III) atom is displaced from the porphyrin mean plane toward the axial ligand. The bridge conformation in **5** is *anti*−*anti* and in **6** *syn*−*anti*.

In this investigation we have employed Mössbauer and EPR spectroscopy as well as magnetization measurements to elucidate the ground-state electronic structures of bridged assemblies **3**−**6**, containing three types of bridges which potentially intervene in certain states of oxidized CcO. The properties determined

(10) Fann, Y. C.; Ahmed, I.; Blackburn, N. J.; Boswell, J. S.; Verkhovskaya, M. L.; Hoffman, B. M.; Wikström, M. *Biochemistry* **1995**, *34*, 10245.
(11) (a) Schoonover, J. R.; Palmer, G. *Biochemistry* **1991**, *30*, 7541. (b) Moody, A. J.; Cooper, C. E.; Rich, P. R. *Biochim. Biophys. Acta* **1991**, *1059*, 189.
(12) Barnes, Z. K.; Babcock, G. T.; Dye, J. L. *Biochemistry* **1991**, *30*, 7597.
(13) (a) Gullo, S. M.; Tayh, J. A.; Li, J.; Baker, G. M. *Arch. Biochem. Biophys.* **1993**, *307*, 78. (b) Cooper, C. E.; Jünemann, S.; Ioannidis, N.; Wrigglesworth, J. M. *Biochim. Biophys. Acta* **1993**, *1144*, 149. (c) Watmough, N. J.; Cheesman, M. R.; Gennis, R. B.; Greenwood, C.; Thomson, A. J. *FEBS Lett.* **1993**, *319*, 151.
(14) Baker, G. M.; Gullo, S. M. *Biochemistry* **1994**, *33*, 8058.
(15) Brown, S.; Moody, A. J.; Mitchell, R.; Rich, P. R. *FEBS Lett.* **1993**, *316*, 216.
(16) (a) Scott, M. J.; Holm, R. H. *J. Am. Chem. Soc.* **1994**, *116*, 11357. (b) Gardner, M. T.; Deinum, G.; Kim, Y.; Babcock, G. T.; Scott, M. J.; Holm, R. H. *Inorg. Chem.* **1996**, *35*, 6878.
(17) Scott, M. J.; Goddard, C. A.; Holm, R. H. *Inorg. Chem.* **1996**, *35*, 2558. OEP = octaethylporphyrinate(2−); Me_5dien = 1,1,4,7,7-pentamethyldiethylenetriamine.
(18) Lee, S. C.; Holm, R. H. *J. Am. Chem. Soc.* **1993**, *115*, 5833, 11789. Me_6tren = tris((dimethylamino)ethyl)amine.
(19) Scott, M. J.; Zhang, H. H.; Lee, S. C.; Hedman, B.; Hodgson, K. O.; Holm, R. H. *J. Am. Chem. Soc.* **1995**, *117*, 568.
(20) Karlin, K. D.; Nanthakumar, A.; Fox, S.; Murthy, N. N.; Ravi, N.; Huynh, B. H.; Orosz, R. D.; Day, E. P. *J. Am. Chem. Soc.* **1994**, *116*, 4753. F_8-TPP = tetrakis(2,6-difluorophenyl)porphyrinate(2−); tmpa = tris(2-pyridylmethyl)amine.
(21) Fox, S.; Nanthakumar, A.; Wikström, M.; Karlin, K. D.; Blackburn, N. J. *J. Am. Chem. Soc.* **1996**, *118*, 24.

are intrinsic to the bridging arrangement and would be expected to apply to the binuclear enzyme site, subject to whatever metric and conformational changes might be imposed on the site by protein structure. In less detailed magnetism experiments, we have previously established the $S = 2$ ground state for **3** and **4**.[18,19] In related work directed toward geometric structure determination, we have developed EXAFS criteria, based on multiple scattering and focusing effects, for linear and nonlinear $Fe^{III}-(OH)-Cu^{II}$ bridges.[19,22]

Experimental Section

Preparation of Compounds. The compounds **1**,[17] **2**,[17] [**3**](ClO_4),[18] [**4**](ClO_4),[19] [**5**](ClO_4),[17] and [**6**]$(ClO_4)_3$[17] were prepared by published methods. For simplicity hereafter, compounds will be referred to by their cation number.

Physical Measurements. Samples for Mössbauer spectroscopy were prepared by placing powdered crystalline solids in Mössbauer cells and suspending the powder in Fisher brand mineral oil (heavy gauge). This procedure prevents alignment of microcrystals in applied magnetic fields. Mössbauer spectra were obtained using a constant-acceleration spectrometer. Isomer shifts are quoted relative to iron metal at 298 K. Magnetic susceptibility measurements were carried out on a MPMS SQUID susceptometer from Quantum Design. Weighed solid samples were placed in gelatin capsules (**4**, **5**) or suspended in Dow Corning high-vacuum grease and placed in gelatin capsules (**1**, **6**). The susceptometer was calibrated with platinum (**4**, **5**) and palladium (**1**, **6**) metal standards for the indicated samples. X-Band EPR spectra were recorded using a Bruker ESP 300 spectrometer equipped with an Oxford Instruments ESR 900 liquid-helium cryostat. Solid samples were suspended in mineral oil, transferred to EPR tubes, and frozen in a liquid-nitrogen bath. Known amounts of **1** were dissolved in Fisher HPLC grade dichloromethane; the solutions were transferred to EPR tubes and frozen in a liquid-nitrogen bath. Mössbauer spectra were fit with eq 1 and magnetization data with eq 2 (vide infra) using computer programs that diagonalize the spin Hamiltonian and perform sums over randomly oriented molecules.

Results

Theoretical Background. The Mössbauer spectra and magnetization data reported below were analyzed with the spin Hamiltonian H (eq 1).[23,24] In eq 2 J describes the exchange

$$H = H_e + H_{HF} \tag{1}$$

$$H_e = J\mathbf{S}_1\cdot\mathbf{S}_2 + D^{Fe}\left\{S_{1z}^2 - \frac{35}{12} + \left(\frac{E^{Fe}}{D^{Fe}}\right)(S_{1x}^2 - S_{1y}^2)\right\} + g_0\beta\mathbf{S}_1\cdot\mathbf{H} + \beta\mathbf{S}_2\cdot\mathbf{g}^{Cu}\cdot\mathbf{H} \tag{2}$$

$$H_{HF} = -g_n\beta_n\mathbf{I}\cdot\mathbf{H} + \mathbf{S}_1\cdot\mathbf{A}\cdot\mathbf{I} + H_Q \tag{3}$$

$$H_Q = \frac{eQV_{zz}}{12}\left\{3I_z^2 - \frac{15}{4} + \eta(I_x^2 - I_y^2)\right\} \tag{4}$$

coupling interaction between the high-spin ferric heme ($S_1 = {}^5/_2$) and the Cu(II) site ($S_2 = {}^1/_2$). The quantities D^{Fe} and E^{Fe} are the zero-field splitting parameters of Fe(III). Because the ^{57}Fe magnetic hyperfine tensor **A** is axial (and generally isotropic) for high-spin ferric hemes, the Mössbauer spectra are very sensitive to E^{Fe}/D^{Fe}.[23c] Our results show that the complexes **3**−**6** have $E^{Fe}/D^{Fe} \leq 0.01$. Therefore, we confine our discussion to the axial case where $E^{Fe}/D^{Fe} = 0$. The other terms in eqs 2−4 describe the electronic Zeeman interactions of high-spin Fe(III) ($g_0\beta\mathbf{S}_1\cdot\mathbf{H}$) and the Cu(II) site ($\beta\mathbf{S}_2\cdot\mathbf{g}^{Cu}\cdot\mathbf{H}$), the quadrupole interaction of the excited state of the ^{57}Fe nucleus with its electronic environment, H_Q, and the ^{57}Fe nuclear Zeeman interaction ($-g_n\beta_n\mathbf{I}\cdot\mathbf{H}$). Other symbols in eqs 2−4 have their usual meanings. Throughout, we will use $g_0 = 2.0$. For coupled systems the influence of the small anisotropies (∼10%) of the Cu(II) **g** tensors is drastically reduced (vide infra); therefore, the data analysis will not be affected in any significant way by assuming $\mathbf{g}^{Cu}$ is isotropic and equal to 2.0.

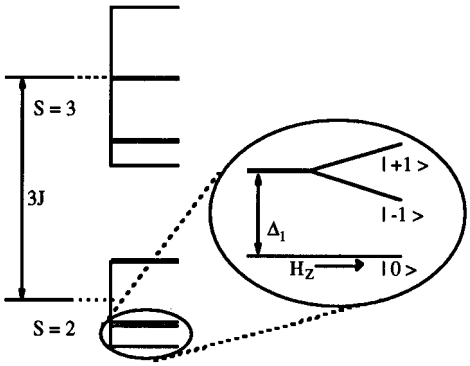

Figure 2. Energy levels resulting from eq 2 for $J > 0$, $D > 0$, $J \gg D$, and $H = 0$. The insert shows the splittings of the lowest three levels of the $S = 2$ multiplet in a magnetic field applied parallel to the z axis.

From our studies we wished to determine, among other parameters, the values of D^{Fe} and J. These parameters are strongly correlated when they have comparable magnitude. For antiferromagnetic coupling, $J > 0$, and for $J \gg D^{Fe}$ the coupled system consists of two multiplets with $S = 2$ and $S = 3$ that are well-separated in energy (Figure 2). Each multiplet exhibits the zero-field splitting $D^{(S)}[S_z^2 - S(S + 1)/3]$. For the $S = 2$ multiplet, $D^{(2)} = (4/3)D^{Fe}$.[23a,b] If J and D^{Fe} have comparable magnitudes, the zero-field splitting term of eq 2 can mix the two multiplets appreciably. For $E^{Fe}/D^{Fe} = 0$, a calculation of D^{Fe} yields the relation

$$D^{Fe} = \frac{\Delta_1}{2}\left(\frac{3J - \Delta_1}{2J - \Delta_1}\right) \tag{5}$$

where Δ_1 is the energy separation between the $M_S = 0$ and $M_S = \pm 1$ levels of the $S = 2$ multiplet (Figure 2). For $J > D^{Fe}$, Δ_1 can be approximated by

$$\Delta_1 \approx \frac{4}{3}D^{Fe}\left\{1 - \frac{2}{9}\left(\frac{D^{Fe}}{J}\right)\right\} \tag{6}$$

In the limit of $J \gg D^{Fe}$, $\Delta_1 = D^{(2)}$.

The x and y components of an applied magnetic field mix the $M_S = \pm 1$ levels into the $M_S = 0$ level. Calculation of the spin expectation values as a function of the magnetic field, **H**, for the ground singlet yields $\langle\mathbf{S}_{1z}\rangle = 0$ and

$$\langle\mathbf{S}_{1x}\rangle = \langle\mathbf{S}_{1y}\rangle = \langle\mathbf{S}_{1\perp}\rangle \approx \frac{-14\beta|\mathbf{H}|}{(\Delta_1^2 + 48\beta^2|\mathbf{H}|^2)^{1/2}} \tag{7}$$

In eq 7 the only unknown quantity is Δ_1. Because the $x-y$ plane is statistically favored for a sample with randomly oriented molecules, and because $|\langle\mathbf{S}_{1\perp}\rangle| \gg |\langle\mathbf{S}_{1z}\rangle|$ at low temperature, the magnetic splitting of the Mössbauer spectra essentially reflects the internal magnetic field in the heme plane, $|\mathbf{H}_{int,\perp}| = |\langle\mathbf{S}_{1\perp}\rangle|A_\perp/g_n\beta_n$. By evaluating $|\mathbf{H}_{int,\perp}|$ as a function of the applied field, Δ_1 can be determined. As can be seen from eq 6, this provides a good initial estimate of D^{Fe}.

(22) Zhang, H. H.; Filipponi, A.; Di Cicco, A.; Lee, S. C.; Scott, M. J.; Holm, R. H.; Hedman, B.; Hodgson, K. O. *Inorg. Chem.* **1996**, *35*, 4819.
(23) (a) Scaringe, R. P.; Hodgson, D. J.; Hatfield, W. E. *Mol. Phys.* **1978**, *35*, 701. (b) Bencini, A.; Gatteschi, *D. EPR of Exchange Coupled Systems*; Springer-Verlag: Berlin, 1990. (c) Münck, E. In *The Porphyrins*; Dolphin, D., Ed.; Academic Press: New York, 1979; Vol. IV, Part B, Chapter 8.
(24) Debrunner, P. G. In *Iron Porphyrins*; VCH: New York, 1989; Part III, Chapter 2.

Table 1. Spin Hamiltonian Parameters of the Compounds Studied

cmpd[a]	J (cm^{-1})	D (cm^{-1})	$A_\perp$ (MHz)	A_z (MHz)	ΔE_Q (mm/s)	δ[e] (mm/s)
1		7.6(7)[b]	−26.7(5)	[−26.7][c]	0.95(3)	0.41(2)
3 (O)	200	4.1(4)	−27.7(5)	−28.8(10)	−1.18(3)	0.48(1)
4 (OH)	170(15)	13.2(20)	−27.9(6)	[−27.9]	1.05(3)	0.41(2)
5 (O_2CH)	18(3)	17(2)	−24.7(5)	−28.1(10)[d]	1.56(2)	0.41(2)
6 ($O_2CH)_2$	−0.30(20)	8.0(10)	−25.5(10)	[−25.5]	1.48(2)	0.44(2)
7[f] (O)	−174	4.5(4)	−27.8(4)	[−27.8]	−1.26(2)	0.44(2)

[a] The appropriate bridging ligand(s) is indicated in parentheses below the sample number. [b] Numbers in parentheses give estimated uncertainties in the least significant digits. [c] Brackets around values for A_z indicate that data were fitted under the assumption that **A** is isotropic. The Mössbauer spectra are sensitive to A_z for $T > 100$ K, provided that the electronic spin fluctuates quickly on the Mössbauer time scale. For some of our samples, intermediate relaxation prevailed for temperatures in the range 100 K $< T <$ 200 K, preventing an accurate determination of A_z. [d] See comments in Discussion. [e] Isomer shift at 4.2 K relative to Fe metal at 298 K. [f] See ref 20.

For the molecules studied here, only the ground state is significantly populated at 4.2 K. At temperatures above 10 K, however, the higher energy levels become populated. In the limit of fast spin relaxation, the internal field at the ^{57}Fe nucleus is given by $\mathbf{H}_{int} = -\langle \mathbf{S}_1 \rangle_{th} \cdot \mathbf{A}/g_n\beta_n$, where $\langle \mathbf{S}_1 \rangle_{th}$ is the thermally averaged expectation value of $\mathbf{S}_1$. For $J < 50$ cm^{-1}, partial population of the $S = 3$ multiplet affects the spin expectation values and, therefore, the magnetic splittings observed in the Mössbauer spectra. Under these conditions, J can be determined by a judicious choice of applied fields and temperature. For larger J values, the Mössbauer spectra yield accurate values for D^{Fe} but become increasingly insensitive to J. Complexes **3** and **4** have large J values ($J \approx 200$ cm^{-1}, vide infra). For both, SQUID magnetization data have been used to determine J. However, because Mössbauer spectroscopy can often sense the presence of monomeric high-spin Fe(III) impurities down to the 2% level, the Mössbauer results are important for the refinement of the analysis of the magnetization data.

The Cu(II) **g** tensor of eq 2 is anisotropic; EPR analyses of the **g** values of the mononuclear complexes **2**, [Cu(Me_6tren)-(O_2CH)](ClO_4),[17] and [Cu(Me_5dien)(OH_2)](ClO_4)$_2$[16a] in frozen solutions show that the anisotropy is less than 10%. While the **g** values of these complexes might closely approximate those in complexes **3**−**6** because of small structural changes on bridge formation, precise values are not required. The Zeeman term of the $S = 2$ multiplet is $\beta\mathbf{S}\cdot\mathbf{g}\cdot\mathbf{H}$, where $\mathbf{g} = {}^7/_6\mathbf{g}_0 - {}^1/_6\mathbf{g}^{Cu}$.[23a,b] Thus, the combined **g** tensor is dominated by the isotropic contribution of the heme ($\mathbf{g}_0 = 2.0$) and any anisotropy in $\mathbf{g}^{Cu}$ is reduced by the spin-coupling factor $^1/_6$.

Mössbauer, EPR, and Magnetization Studies. Values of isomer shifts (δ), quadrupole splittings (ΔE_Q), hyperfine coupling constants (A_i), zero-field splittings (D^{Fe}), and exchange interactions (J) for compounds **1** and **3**−**6**, obtained from analysis of spectroscopic and magnetic data, are collected in Table 1.

(a) Heme Complex 1. The Mössbauer spectra of **1** recorded in zero field (A) and in applied fields of 2.0 T (B) and 8.0 T (C) are shown in Figure 3. The zero-field spectrum is fit with $\Delta E_Q = 0.94$ mm/s and $\delta = 0.41$ mm/s. These Mössbauer parameters are typical of a high-spin Fe(III) porphyrin.[24] The sharpness of the absorption lines at 8.0 T shows that all orientations for which the applied field is in the $x-y$ (heme) plane are equivalent, implying that $E^{Fe}/D^{Fe} = 0$, $A_x = A_y$, and $\eta = 0$. The conclusion $E^{Fe}/D^{Fe} = 0$ is supported by the observation of a sharp axial feature at $\mathbf{g}_\perp = 6.0$ in the EPR spectrum of **1** in dichloromethane solution (Figure 4). The poor signal/noise ratio results from the requirement that [**1**] < 10 μM is necessary in order to avoid spin−spin interactions. At high concentrations we have observed signals (not shown) that indicate spin−spin interactions between neighboring molecules. Weak intermolecular couplings were also found in the EPR spectrum of polycrystalline **1**. Such interactions are also suggested in the low-field Mössbauer spectra of polycrystalline samples; however, applied fields ≥2.0 T seem sufficient to decouple these interactions.

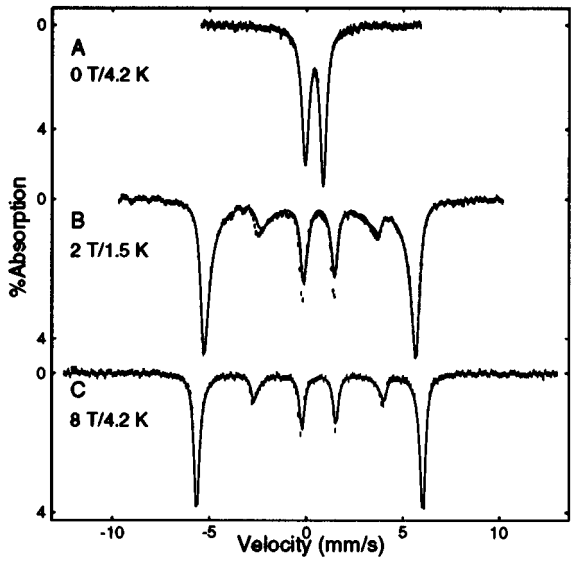

Figure 3. Mössbauer spectra of heme complex **1** recorded at 4.2 K in zero field (A) and applied magnetic fields of 2.0 T (B) and 8.0 T (C). The solid lines are theoretical spectra computed in the limit of fast relaxation from eq 1 for $J = 0$ and $S_2 = 0$ and using the parameters listed in Table 1. The lines of the zero-field spectrum are broadened due to relaxation of the electronic spin.

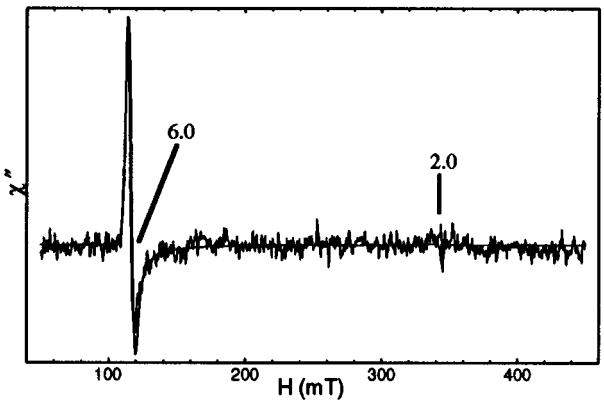

Figure 4. X-Band EPR spectrum of heme complex **1** in dichloromethane. The poor signal/noise results from the requirement that the concentration of **1** be kept low; for [**1**] > 10 mM the EPR spectra display spin−spin splittings. Conditions: [**1**] = 5 μM, $T \approx 4.2$ K, microwave power 20 mW, frequency 9.65 GHz.

The Mössbauer data of **1** have been supplemented by magnetization studies at four magnetic fields in the interval 0.5−5.0 T over the temperature range 2−300 K.[25] The data and theoretical fits are presented in Figure 5. When they are taken together, the Mössbauer and magnetization data yield the zero-

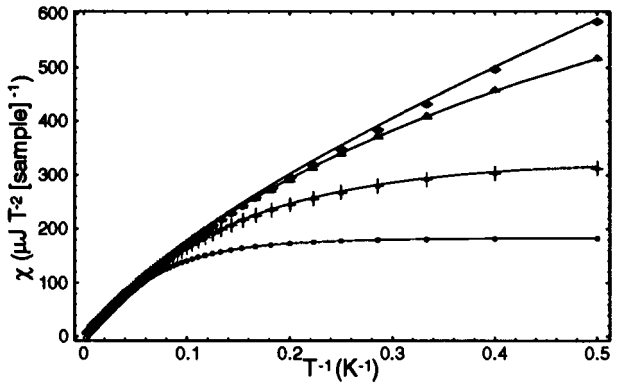

Figure 5. Magnetization behavior of polycrystalline **1** (♦, 0.5 T; ▲, 1.0 T; +, 2.5 T; ●, 5.0 T). Solid lines are theoretical curves computed from eq 2 for $S_1 = {}^5/_2$ and $S_2 = 0$. Curves are drawn for $D^{Fe} = 7.5$ cm^{-1} and an intermolecular coupling of 0.025 cm^{-1} between neighboring molecules.

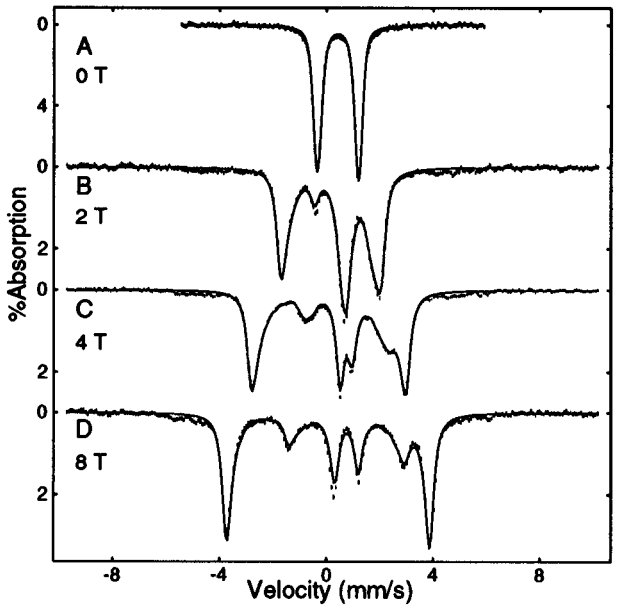

Figure 6. Mössbauer spectra of formate-bridged **5** at 4.2 K. Spectra were recorded for a polycrystalline sample in the indicated applied magnetic fields. The sample contained a contaminant, accounting for *ca*. 13% of the total iron and attributed to **4**. Absorption by this contaminant is apparent at Doppler velocities $|v| > 4$ mm/s. The solid lines are theoretical spectra computed from eq 1, in the fast relaxation limit, using the parameters in Table 1.

field splitting $D^{Fe} = +7.6$ cm^{-1}. The fits to the Mössbauer spectra yield $A_x = A_y = -26.4$ MHz. The data are quite insensitive to A_z because the magnetic anisotropy favors sampling of the $x-y$ plane at low temperatures, whereas intermediate relaxation leads to a deterioration of the resolution at temperatures (>100 K) where the spectra would be sensitive to A_z.

(b) Formate-Bridged Assembly 5. A series of Mössbauer spectra for **5** are set out in Figures 6 and 7. The spectra of Figure 6 probe the electronic system at 4.2 K as a function of applied field, whereas those of Figure 7 were recorded at a constant field of 8.0 T between 25 and 150 K. The solid lines

(25) Low magnetic field saturation magnetization could be fit well by assuming that nearest-neighbor interactions involve only one neighboring molecule. Indeed, the crystal structure of **1** shows that the molecules exist in pairs with the plane of the porphyrin rings parallel and faced back-to-back at a separation of 3.63 Å and an average Fe−Fe distance of 5.65 Å.[17] The strength of the intermolecular exchange coupling is small ($J < 0.05$ cm^{-1}) and antiferromagnetic, suggesting non-zero orbital overlap between the porphyrin rings.

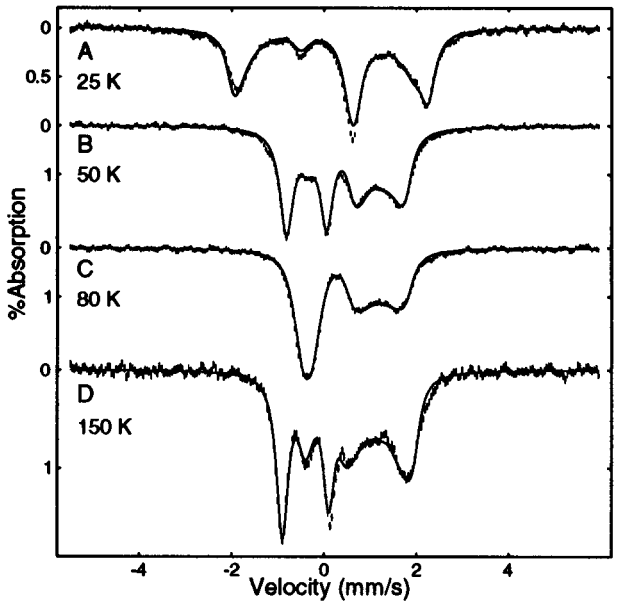

Figure 7. Mössbauer spectra of polycrystalline **5** recorded at a fixed field of 8.0 T at the temperatures indicated. The solid lines are theoretical curves computed, in the fast relaxation limit, from eq 1 using the parameters in Table 1. The contribution of the contaminant (13% of total iron) has been removed from the data using the data for **4** (Figure 9).

in both figures are simulations of the data using the parameter set of Table 1. We briefly note how some of the parameters were determined. First, the spectra of Figure 6 contain contaminants that contribute absorption at velocities at $|v| > 4$ mm/s. Their Mössbauer features suggest that they are mainly or exclusively **1** and **4**. Because these impurities contribute less than 8% of the total iron, they do not interfere with interpretation of the spectra of **5**. Therefore, this contribution has not been subtracted from the spectra of Figure 6. The spectra of Figure 7 were taken from a different preparation of **5**[26] and analyzed after subtraction of a 13% contribution of **4**, using an experimental spectrum of **4** obtained under exactly the same conditions of temperature and magnetic field. The contribution of **1** to the spectra of Figure 7 was negligible. Second, as pointed out above, the low-temperature Mössbauer spectra are sensitive to Δ_1 rather than to J and D^{Fe} separately. From fits to the 4.2 K spectra, we obtained $\Delta_1 = 18(1)$ cm^{-1} and $A_x = A_y = -24.4$ MHz. From the variable-temperature data, especially the 8.0 T spectrum at 50 K, we determined that J is positive and is confined to the range 15−30 cm^{-1}. Third, the 150 K spectrum of Figure 7 consists of a low-energy triplet and a high-energy doublet feature (showing that $\Delta E_Q > 0$). Because the electric field gradient tensor is axial ($\eta = 0$, established at 4.2 K), the splitting of the low-energy triplet is sensitive to A_x and A_y, whereas the splitting of the high-energy feature depends on A_z. While the value $A_\perp = -24.4$ MHz produces the correct splittings for the low-energy feature, it was necessary to use $A_z = -28$ MHz to simulate the high-energy feature. Thus, the **A** tensor of the high-spin Fe(III) site of **5** is anisotropic and $|A_z| > |A_\perp|$.

In order to obtain tighter bounds on D^{Fe} and J, we have studied the magnetization of polycrystalline **5**. The 5.0 T data and a fit are shown in Figure 8B. These data are best fit with $15 < J < 20$ cm^{-1}. When they are taken together, the Mössbauer and magnetization data suggest $D^{Fe} = 17$ cm^{-1} and

(26) The presence of impurities in samples of **5** is not unexpected. No satisfactory method of purification of this compound by recrystallization could be found; in its preparation, crystals of **5** were manually separated from impurities.[17]

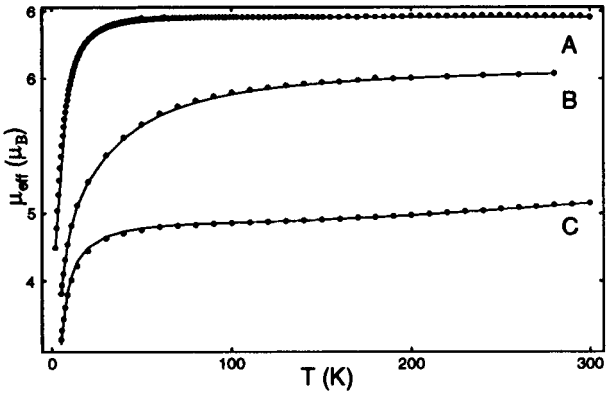

Figure 8. Temperature dependence of the magnetic susceptibilities of polycrystalline **1** (A), oxo-bridged **5** (B), and hydroxo-bridged **4** (C) recorded at fields of 5.0 T (**1**, **5**) and 0.5 T (**4**). Points are experimental data; solid lines represent best fits to the data with the limits of uncertainty reported in Table 1.

$J = 18$ cm^{-1}. It is noteworthy that the zero-field splitting parameter D^{Fe} for bridged assembly **5** is substantially larger than that for heme complex **1.**[27]

(c) Oxo-Bridged Assembly 3 and Hydroxo-Bridged Assembly 4. We have shown earlier that the Fe(III) and Cu(II) sites of **3** are strongly antiferromagnetically coupled such that the susceptibility follows the Curie−Weiss law at 4−300 K.[18] From these results it was estimated that $J \geq 200$ cm^{-1}. Analysis of the magnetic susceptibility data of **4** (Figure 8C) has demonstrated strong antiferromagnetic coupling in this complex as well, with $J = 170$ cm^{-1}. The Mössbauer spectra of both complexes, presented in Figures 9 (**4**) and 10 (**3**), are insensitive to J and were readily analyzed in the strong coupling limit. One observation is especially noteworthy. As indicated above, the axial nature of the Hamiltonian of high-spin Fe(III) hemes renders their low-temperature spectra quite insensitive to the z component of the magnetic hyperfine tensor. Nonetheless, we have been able to determine the A_z value of **3**. This complex has the relatively small value $D^{Fe} = 4.1$ cm^{-1}, and therefore, the $M_S = \pm 1$ levels of the $S = 2$ ground state are at the energy $\Delta_1 = D^{(2)} = {}^4/_3 D^{Fe} = 5.5$ cm^{-1}. The two excited states split readily in an applied field, producing sizeable magnetization along the z axis; $|\langle \mathbf{S}_z \rangle| = 1$ and $|\langle \mathbf{S}_x \rangle| = |\langle \mathbf{S}_y \rangle| \approx 0$ in fields of moderate strength. The $M_S = -1$ state, which produces a hyperfine field along the z axis, $\mathbf{H}_{int,z} = +A_z/g_n\beta_n$, is lowered in energy and becomes populated at 4.2 K. In the slow relaxation limit, the $M_S = 0$ and $M_S = -1$ states produce separate Mössbauer spectra with intensities according to the Boltzmann distribution. The contribution of the $M_S = -1$ level is indicated by the arrows in the 4.2 K spectrum of Figure 10; as can be seen from inspection of Figure 10C, this state is depopulated at 1.5 K. By fitting the splitting of the $M_S = -1$ level, $A_z = -28.8$ cm^{-1} was determined for **3**. (Broadening due to intermediate spin relaxation prevented the determination of A_z at higher temperature.) Note that the Mössbauer spectra are sensitive to D^{Fe} in two different ways. First, the magnetic splitting of the ground-state Mössbauer spectrum is determined by mixing the $M_S = \pm 1$ excited states into the ground state by in-plane components of the applied field. Second, the relative populations of the $M_S = 0$ and $M_S = -1$ levels (Figure 2) are determined by D^{Fe} as observed in the spectrum of Figure 10B.

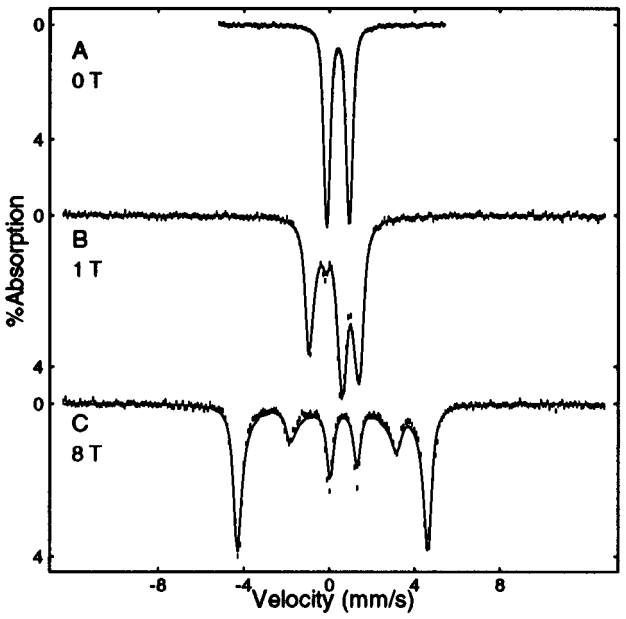

Figure 9. Mössbauer spectra of hydroxo-bridged **4** recorded in zero field (A) and in applied fields of 1.0 T (B) and 8.0 T (C). The solid lines are theoretical curves calculated in the fast relaxation limit based on eq 1 using the parameters in Table 1.

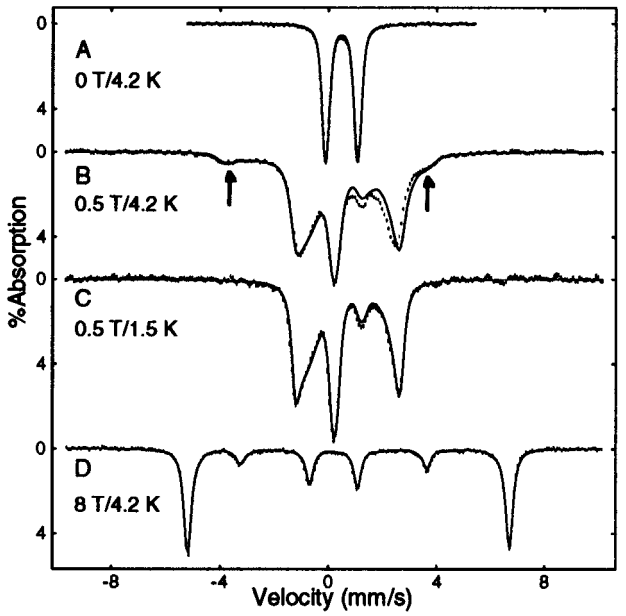

Figure 10. Low-temperature Mössbauer spectra of oxo-bridged **3** recorded at the fields and temperatures indicated. The solid lines are theoretical spectra computed in the slow relaxation limit from eq 1 using the parameters in Table 1. The arrows in (B) point out the contribution of the $M_S = -1$ level (see Figure 1), which is populated to *ca*. 10% at 4.2 K and 0.5 T applied field. At 1.5 K (C) the $M_S = -1$ level is depopulated. The mismatch between theory and experiment in (B) is attributable to the onset of fast spin relaxation in the $x-y$ plane.

(d) Trinuclear Doubly Bridged Assembly 6. The zero-field spectrum of doubly formate bridged **6**, shown in Figure 11, consists of a doublet with $\Delta E_Q = 1.48$ mm/s and $\delta = 0.44$ mm/s, values indicative of a high-spin Fe(III) heme. X-Band EPR spectra of the polycrystalline material[28] revealed very broad

(27) We are aware of the possible question as to whether the magnetization data of **5** are affected by presence of the contaminant **4**. The material used for the study of **5** was a later batch, prepared with particular emphasis on avoiding contamination by **4**. Note from Figure 8C that the magnetic susceptibility of **4** increases at $T > 100$ K because the $S = 3$ state becomes thermally populated. Thus, we can take the relative "flatness" of the plot for **5** (Figure 4B) as a measure of the absence of **4**. Moreover, because Mössbauer spectroscopy has already suggested the range 15 cm^{-1} < J < 30 cm^{-1} for **5**, the influence of **4** on on the determination of J from magnetic susceptibility is practically negligible inasmuch as the J value of **5** is primarily determined by data in the 10−70 K range. In fact, sample contamination as large as the mole ratio **4**:**5** = 0.15:1 still permits the conclusion 15 cm^{-1} < J < 20 cm^{-1}.

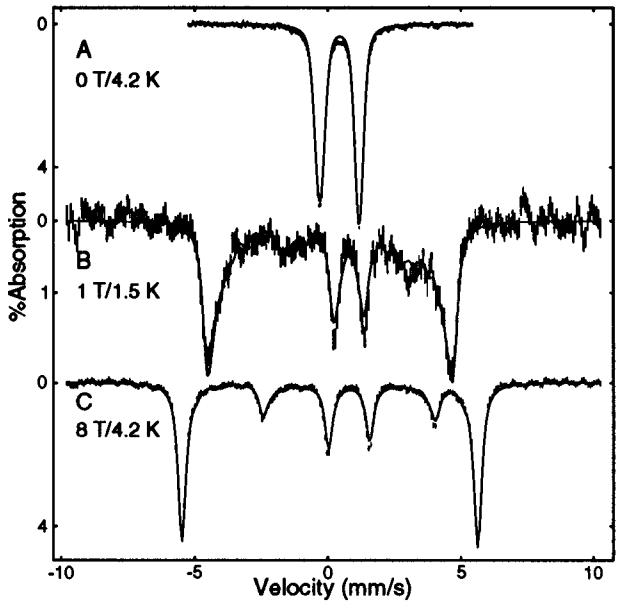

Figure 11. Mössbauer spectra of trinuclear **6** at 4.2 K in zero field (A) and 8.0 T (C). Spectrum B was collected under the conditions of 1.5 K and 1.0 T. The solid line in (C) is a theoretical spectrum simulated for a monomeric high-spin Fe(III) site using the parameters listed in Table 1. For the 1.0 T spectrum, the same parameters were employed together with the molecular field correction of eq 9, using $J = -0.22$ cm^{-1}. Theoretical spectra were calculated in the fast relaxation limit.

unresolved features indicative of intermolecular interactions and did not permit determination of the ground spin state from the spectrum.

Given the results for formate-bridged **5**, a spin-coupled system is expected for **6**, which because of its centrosymmetry will have identical exchange interactions between the two Cu(II) sites and the axial Fe(III) site ($E^{Fe}/D^{Fe} = 0$). These circumstances suggest the following Hamiltonian for the electronic system of **6**:

$$H_e = J\mathbf{S}_1\cdot(\mathbf{S}_2 + \mathbf{S}_3) + D^{Fe}\left\{S_{1z}^{\,2} - \frac{35}{12}\right\} + g_0\beta\mathbf{S}_1\cdot\mathbf{H} + g^{Cu}\beta(\mathbf{S}_2 + \mathbf{S}_3)\cdot\mathbf{H} \quad (8)$$

In the limit of strong exchange couplings, the ground state of the coupled system will have $S = {}^7/_2$ for ferromagnetic coupling and $S = {}^3/_2$ for antiferromagnetic coupling. For weak coupling, $|J| \ll D^{Fe}$, the magnetic susceptibility of **6** will behave nearly like an uncoupled system consisting of two Cu(II) ($S = {}^1/_2$) and Fe(III) ($S = {}^5/_2$). The solid lines in Figure 12 are theoretical curves for the temperature dependence of the effective magnetic moment μ_{eff} for the three limiting cases, assuming $g_0 = g^{Cu} = 2.0$. The data for polycrystalline **6**, recorded in a magnetic field of 5.0 T, saturate at $\mu_{eff} \approx 6.4\ \mu_B$, showing that J must be relatively small. Using a program that computes the powder susceptibility for the three-spin problem of eq 8, the magnetization data of Figure 13 have been fit using $D^{Fe} = 8.0$ cm^{-1} and $J = -0.42$ cm^{-1}.

These results are independently confirmed by Mössbauer data. The 8.0 T Mössbauer spectrum of **6**, provided in Figure 11, exhibits sharp absorption features, showing that the system is axial ($E^{Fe}/D^{Fe} = 0$, $A_x = A_y$, $\eta = 0$). Because J is small, the 8.0 T spectrum could be readily fit for the uncoupled case, i.e. with a spin Hamiltonian appropriate to mononuclear high-spin Fe(III). However, spectra recorded in fields below 3.0 T are not well-fit with this assumption. For instance, the 1.0 T spectrum of Figure 11B, recorded at 1.5 K, displays a splitting expected for a spectrum at 1.1 T. This deviation can be understood by taking into account the weak exchange coupling of Fe(III) with the two Cu(II) sites. This has been done by modifying eq 8 by treating the exchange interaction with the Cu(II) sites in a molecular field approximation. The spin operators of the Cu(II) sites in the exchange term of eq 8 were replaced by their expectation values taken in the limit $J = 0$ but retaining the spin operator $\mathbf{S}_1$ of Fe(III):

$$H_e = D^{Fe}\left\{S_{1z}^{\,2} - \frac{35}{12}\right\} + 2\beta\left\{|\mathbf{H}| - \left|\langle\mathbf{S}_i^{Cu}\rangle_{th}\frac{J}{\beta}\right|\right\}\mathbf{S}_1\cdot\mathbf{e} \quad (9)$$

where $\mathbf{H} = |\mathbf{H}|\mathbf{e}$.

At 1.5 K and 1.0 T, the thermally averaged expectation value $|\langle\mathbf{S}_i^{Cu}\rangle_{th}|$ is isotropic and computed to be 0.21. Therefore, the Hamiltonian at this field and temperature can be written as eq 10. Note that the correction term in (10) adds to the applied

$$H_e = D^{Fe}\left\{S_{1z}^{\,2} - \frac{35}{12}\right\} + 2\beta\{|\mathbf{H}| - 0.45J\}\mathbf{S}_1\cdot\mathbf{e} \quad (10)$$

field for *ferromagnetic* coupling ($J < 0$). The fit shown in Figure 11B was obtained for $J = -0.22$ cm^{-1} ($-0.45J = 0.10$ T). This result confirms our analysis of the magnetization data and establishes J to be between -0.1 and -0.5 cm^{-1}.

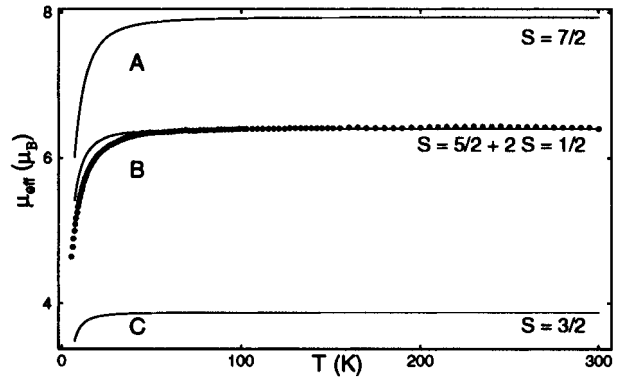

Figure 12. Temperature dependence of the magnetic susceptibility of trinuclear **6** measured at 5 T. The solid lines are 5 T theoretical curves ($D = 0$) for three limiting cases: (A) an $S = {}^7/_2$ ground state resulting from strong ferromagnetic coupling of the Fe(III) and two Cu(II) sites, (B) a weakly coupled system ($|J| \ll D^{Fe}$), and (C) an $S = {}^3/_2$ ground state resulting from strong antiferromagnetic coupling of the three sites. The points are experimental data. The plot clearly identifies (B) as the correct description of the coupling interaction.

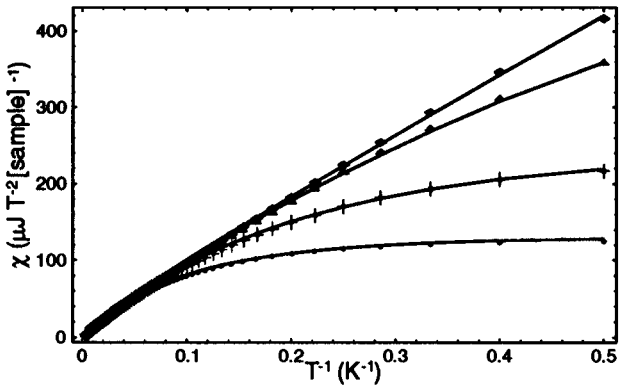

Figure 13. Magnetization behavior of trinuclear **6** (♦, 0.5 T; ▲, 1.0 T; +, 2.5 T; ●, 5.0 T). Solid lines are theoretical curves that result from computing the powder susceptibility with the three-spin coupling Hamiltonian of eq 8 using $D^{Fe} = 8.0$ cm^{-1}, $J = -0.42$ cm^{-1}, and $g^{Cu} = 2.0$.

(28) Complex **6** dissociates in solution.[17]

Discussion

This investigation has focused on the electronic structure of bridged heme-based $Fe^{III}-X-Cu^{II}$ molecular assemblies with $X = O^{2-}$, OH^-, and HCO_2^-. Mössbauer and EPR spectroscopy and magnetic susceptibility have been used to determine exchange-coupling parameters as well as ^{57}Fe hyperfine parameters. When the same sample was studied with multiple techniques, the accuracy of the parameter sets in Table 1 was significantly improved. For instance, the Mössbauer data established that the rhombicity parameter of the zero-field splitting is approximately zero ($0 \leq E^{Fe}/D^{Fe} \leq 0.01$) for all complexes studied. This constraint was applied to an analysis of the magnetization data.

Until such time as the nature of bridged heme a_3-Cu_B sites is structurally established for oxidases, our understanding of the electronic structures and exchange interactions of heme-based $Fe^{III}-X-Cu^{II}$ bridges must of necessity be derived from synthetic molecules of known structure. With the information now available, electronic properties within the set of synthetic complexes can be compared, and considerations of these properties in the context of information about heme−copper oxidases can be offered.

Comparative Electronic Properties of Bridged Assemblies. Summarized in Table 1 is the body of electronic structural information obtained for complexes prepared and studied in these laboratories. Also included are data for oxo-bridged **7** studied by Karlin and co-workers.[20,21] First, note the differences between the oxo- and hydroxo-bridged complexes. The isomer shifts of **3** and **7** are 0.05−0.07 mm/s higher than that of **4**, a reflection of the electron-rich oxo bridge. Furthermore, the sign of ΔE_Q for both **3** and **7** is negative, opposite to that of **4**, and the zero-field splittings of the oxo-bridged species are considerably smaller. While these differences are drawn from only three compounds, it would appear that linear oxo and nonlinear hydroxo bridges are distinguishable by their values of δ, ΔE_Q, and D^{Fe}. Second, it is useful to observe the magnitude of the antiferromagnetic exchange coupling constant. Together with information from earlier work,[18] a series of types of bridging ligands can be shown to have increasing J values, $J(HCO_2^-) < J(OH^-) \leq J(O^{2-})$. Note that the Cu(II) magnetic orbital is not the same in all complexes, being $\sigma^*(d_{z^2})$ when the copper fragment is trigonal bipyramidal as in the oxo-bridged complexes (**3**, **7**) and $\sigma^*(d_{x^2-y^2})$ in the distorted-square-pyramidal cases (**4**, **5**). However, both orbitals overlap directly with bridge atom orbitals to create an exchange pathway.[29,31] The J value of any formate-bridged assembly will depend to some extent on the bridge conformation. However, with the J value of **5** being an order of magnitude less than that of **4**, it follows that formate is intrinsically a less effective propagator of exchange interactions than hydroxo in any of the three stereochemically possible μ-η^1:η^1 formate arrangements (*syn*−*syn*, *syn*−*anti*, *anti*−*anti*).[17] Thus far, we have been unable to isolate, for direct comparison, oxo- and hydroxo-bridged species with the same Cu(II) fragment. Complex **7** has a structurally analogous bridge and a trigonal-bipyramidal Cu(II) fragment.[20] Its strong exchange-coupling ($J = 174$ cm^{-1}) is comparable with those of both **3** and **4**, indicating that as yet no distinction can be made between $X = O^{2-}$ and OH^- bridges in $Fe^{III}-X-Cu^{II}$ assemblies on the basis of J values. This species can be reversibly protonated to hydroxo-bridged **8**, whose bridge distances and angle (157 ± 5°) are close to those of **4**; magnetic properties have not been reported.

Bridged Assemblies and Heme a_3-Cu_B Sites. (a) Oxo and Hydroxo Bridged. The binuclear site of oxidized bovine heart CcO has $\Delta E_Q = +1.0$ mm/s and $\delta = 0.41$ mm/s at 4.2 K,[32] and the cytochrome oxidase from *Thermus thermophilus* shows $\Delta E_Q = +1.10$ mm/s and $\delta = 0.41$ mm/s.[33] We note that these values are in very close agreement with those of **4** (Table 1) but recognize that these parameters are not highly sensitive to different axial monoanions. Further, as observed previously,[20] the *negative* sign of ΔE_Q for **3** and **7** is opposite to that found for the enzymes,[34] a result that militates against a native oxo bridge with the metric parameters of **3** and **7**. The value $J = 170$ cm^{-1} for **4** is consistent with the observation of Curie dependence of the susceptibility of oxidized CcO corresponding to an $S = 2$ ground state.[3,4] As noted at the outset, the *B. subtilis* oxidase has an oxygenous ligand with an exchangeable proton which ENDOR spectroscopy has shown to be associated with Cu_B.[10] To our knowledge, no EXAFS spectrum of an oxidized cytochrome oxidase exhibits the multiple scattering focusing effects known to occur when the an intervening atom is placed linearly between photoabsorber and backscatterer, resulting in a large enhancement in the EXAFS signal.[19,21,22] We conclude that the collective evidence now available favors the nonlinear $Fe^{III}-(OH)-Cu^{II}$ bridge in the oxidized form of the cytochrome oxidases.

(b) Formate Bridged. Oxidized formate-bound bovine heart CcO and *E. coli* cytochrome *bo* yield EPR signals with effective g values centered around $g = 12$ and 2.95[35] and $g = 13$ and ~2.8,[13c] respectively. These signals are similar to those observed for the noninhibited slow form of the bovine heart enzyme.[35] From a variety of spectroscopic studies,[35,36] it has been proposed that these resonances originate from transitions between sublevels of an $S = 2$ multiplet. Using saturation magnetization studies, Day *et al.*[4] have reported a negative zero-field splitting ($D = -7$ cm^{-1}) and large rhombicities ($E/D = 0.27$) for the slow form of bovine heart CcO.[37] In contrast, the Mössbauer studies of **5** show that the zero-field splitting of the $S = 2$ multiplet is highly axial and unusually large (Table 1). For these parameters and under the condition $\beta H \ll D$[2], the $S = 2$ multiplet will not yield an EPR signal. Indeed, we have failed to observe an EPR resonance for **5** at X-band frequencies in either the parallel or perpendicular mode. In assessing this result in the context of CcO, it should be kept in mind that heme a_3, although high-spin, is most likely six- rather than five-coordinate owing to the presence of a histidyl residue[5,6] distal to any possible formate bridge. Complex **5** contains a five-coordinate heme group. Complex **6**, with two formate bridges and extremely weak coupling, is evidently not biologically relevant and is not further considered in this context.

(29) On the basis of magnetic susceptibility data (4−300 K), $[(OEP)Fe-F-Cu(bnpy_2)]^{2+}$ [30] is not exchange-coupled.[18] However, fluoride cannot be placed in the above series because the $\sigma^*(d_{x^2-y^2})$ magnetic orbital of the square-pyramidal Cu(II) fragment is nearly orthogonal to the exchange-propagating orbitals of the bridging fluoride atom.

(30) Lee, S. C.; Holm, R. H. *Inorg. Chem.* **1993**, *32*, 4745. $bnpy_2$ = bis-(2-pyrid-2-ylethyl)benzyamine.

(31) Exchange pathways using both σ^* Cu(II) orbitals in $Fe^{III}-X-Cu(II)$ bridges have been briefly depicted: Kahn, O. *Struct. Bonding (Berlin)* **1987**, *68*, 89.

(32) Kent, T. A.; Münck, E.; Dunham, W. R.; Filter, W. F.; Findling, K.; Yoshida, T.; Fee, J. A. *J. Biol. Chem.* **1982**, *257*, 12489.

(33) Kent, T. A.; Young, L. J.; Palmer, G.; Fee, J. A.; Münck, E. *J. Biol. Chem.* **1983**, *258*, 8543.

(34) Rusnak, F. M.; Münck, E.; Nitsche, C. I.; Zimmermann, B. H.; Fee, J. A. *J. Biol. Chem.* **1987**, *262*, 16328.

(35) Cooper, C. E.; Salerno, J. C. *J. Biol. Chem.* **1992**, *267*, 280.

(36) (a) Brudwig, G. W.; Morse, R. H.; Chan, S. I. *J. Magn. Reson.* **1986**, *67*, 189. (b) Hagen, W. R.; Dunham, W. R.; Sands, R. H.; Shaw, R. W.; Beinert, H. *Biochim. Biophys. Acta* **1984**, *765*, 399. (c) Dunham, W. R.; Sands, R. H.; Shaw, R. W.; Beinert, H. *Biochim. Biophys. Acta* **1983**, *748*, 73. (d) Brudwig, G. W.; Stevens, T. W.; Morse, R. H.; Chan, S. I. *Biochemistry* **1981**, *20*, 3912.

Comparison of the X-ray structures of **1** and **5** shows differences in the environments of the Fe(III) atoms.[17] In **5**, Fe(III) is 0.08 Å closer to the mean porphyrin plane and the Fe−O bond has increased by 0.06 Å relative to **1**. This observation suggests that the parameters of **1** are not transferable to the coupled system **5**. The data of Table 1, which show a substantial increase in D^{Fe} and ΔE_Q for the bridged complex, confirm the nontransferability. To our knowledge, $D^{Fe} = 17$ cm^{-1} is the largest value reported for any Fe(III) heme complex.

A large zero-field splitting parameter indicates that the $^6A_1$ ground state of Fe(III) has substantial admixtures from excited spin quartets. Maltempo[38] has proposed an electronic model that considers mixing of an excited $^4A_2$ state (at energy Δ) with the $^6A_1$ ground manifold by spin−orbit coupling. (In predominantly C_{4v} symmetry, the $^4A_2$ configuration results when a $d_{x^2-y^2}$ electron of the high-spin configuration is transferred to the d_{xy} orbital of the t_{2g} set.) In this model, the parameter D^{Fe} is given by $D^{Fe} = \xi^2/5\Delta$, where ξ is the one-electron spin−orbit coupling constant. Assuming the free-ion value of ξ (400 cm^{-1}) and taking $D^{Fe} = 17$ cm^{-1} for **5**, the model yields $\Delta = 1900$ cm^{-1}. For these values, the Maltempo model predicts energies for the $M_S = \pm^1/_2$, $\pm^3/_2$, and $\pm^5/_2$ doublets that deviate somewhat from those predicted by the $S = ^5/_2$ Hamiltonian, $H = D^{Fe}[S_z^2 - S(S + 1)/3]$. Whereas the spin Hamiltonian yields $\Delta_2/\Delta_1 = 2$, where $\Delta_2 = E_{\pm5/2} - E_{\pm3/2}$ and $\Delta_1 = E_{\pm3/2} - E_{\pm1/2}$, the Maltempo model yields $\Delta_2/\Delta_1 = 2.11$. For a mononuclear Fe(III) site, the effects of mixing the $^4A_2$ state into the $^6A_1$ manifold are readily expressed in the framework of an effective $S = ^5/_2$ Hamiltonian. Gismelseed and co-workers[39] have given expressions which show that the effective magnetic hyperfine interactions along the *z* axis will *decrease* relative to those in the *x*−*y* plane. Thus, the Maltempo model predicts anisotropies in **A** opposite to those observed for **5**. For an exchange-coupled Fe(III)−Cu(II) system, the Maltempo model can be incorporated by considering the Hamiltonian (11), where the spin−orbit coupling and the Zeeman interactions of the Fe(III) site are evaluated in the 10×10 basis of the $^6A_1$ and $^4A_2$ manifolds.[40] The $\delta_{3/2,S_1}$ term is the Kronecker symbol. By diagonalization of eq 11, we have computed the internal fields along the *z* axis and in the *x*−*y* plane. Our calculations show that the Maltempo model cannot reproduce the observed anisotropy $|A_z| > |A_\perp|$, and we conclude than an electronic model with an extended basis, perhaps involving vibronic interactions,[41] needs to be considered.

$$H_e = J\mathbf{S}_1\cdot\mathbf{S}_2 + \beta\mathbf{S}_2\cdot\mathbf{g}^{Cu}\cdot\mathbf{H} + \Delta\delta_{3/2,S_1} + \sum_{i=1}^{5}\{\xi\mathbf{l}_i\cdot\mathbf{s}_i + \beta(\mathbf{l}_i + 2\mathbf{s}_i)\cdot\mathbf{H}\} \quad (11)$$

While the electronic structural description of **5** may require some further refinement, this complex has nonetheless conveyed significant information. Formate-bound bovine heart CcO follows the Curie law between 20 and 180 K with the magnetic moment $\mu_{eff}^2 = 36.6\ \mu_B^2$.[12] After we subtract the contribution of the $S = ^1/_2$ Cu_A and heme *a* sites, $\mu_{eff}^2 = 24.0\ \mu_B^2$ for the binuclear site. Inasmuch as heme a_3 has been independently established as high-spin by spectroscopy,[42] the magnetism is only accountable in terms of an antiferromagnetically coupled $S = 2$ ground state.[12] As noted above, formate possesses three geometric binding modes when utilizing both oxygen atoms; the *anti*−*anti* mode of **5** may, of course, not apply to a putative formate bridge in an enzyme. While conformational differences will affect magnetic parameters, it is highly improbable that any different μ-η^1:η^1 conformation of **5** would change *J* by an order of magnitude, thus making it comparable with the value for **4**. Clearly the estimate $J \geq 400$ cm^{-1} cannot be rationalized for formate-bound CcO with the magnetic behavior of **5**, which is decidedly non-Curie (Figure 8B). Further, given the similar strongly coupled magnetic behavior of the fast, slow, and formate-bound forms of the enzymes, it is most unlikely that the slow form contains an endogenous μ-η^1:η^1 carboxylate bridge. If formate or endogenous carboxylate does bridge at all, the μ-η^2 mode (utilizing a single oxygen atom) appears more probable. In such a case, an exchange coupling approximating that in **4** may result.

Acknowledgment. We wish to acknowledge Dr. Emile Bominaar for his contributions in developing an electronic theory to describe a high-spin Fe(III). We also thank Dr. Lawrence Que, Jr., for allowing us the use of his facilities in acquiring the magnetization data presented here on solid samples of **4** and **5**. This research was supported at Carnegie Mellon University by NIH Grant GM 22701 and at Harvard University by NSF Grant CHE 94-23830.

IC960826V

(37) It should be noted that the Mössbauer spectra of the a_3-Cu_B site of oxidized *Thermus thermophilus* c_1aa_3 can be simulated equally well in terms of weak ($J \approx 1$ cm^{-1}) and strong ($J \geq 7$ cm^{-1}) coupling.[34] Moreover, the Mössbauer spectra show that $E/D < 0.05$. The small E/D value suggests the absence of an integer spin EPR signal for cytochrome c_1aa_3. Indeed, no such signal has been reported for this enzyme. The E/D value of oxidized cytochrome c_1aa_3 oxidase falls into the range of small E/D values ($0 \leq E/D \leq 0.08$) that are typical for ferric porphyrins and contrasts with the large rhombicities deduced from fits of the magnetization data of the bovine heart enzyme. The Mössbauer data of cytochrome c_1aa_3 reveal the presence of multiple high-spin ferric forms. Multiple forms (in addition to the kinetically distinguishable slow and fast forms) may exist for the bovine heart enzyme. In fact, the X-ray structure of the bovine enzyme, in contrast to the frozen-solution EXAFS data, suggests the absence of a bridging ligand (r(Fe-Cu_B) = 5.2 Å from the X-ray analysis as opposed to r(Fe-Cu_B) = 3.96 Å from EXAFS) This suggests that the single crystals of the bovine heart enzyme will display an $S = 5/2$ EPR signal.

(38) (a) Maltempo, M. M. *J. Chem. Phys.* **1974**, *61*, 2540. (b) Maltempo, M. M.; Moss, T. H. *Q. Rev. Biophys.* **1976**, *9*, 181.

(39) Gismelseed, A.; Bominaar, E. L.; Bill, E.; Trautwein, A. X.; Winkler, H.; Nasri, H.; Doppelt, P.; Mandon, D.; Fisher, J.; Weiss, R. *Inorg. Chem.* **1990**, *29*, 2741.

(40) Kauffmann, K. E. Ph.D. Thesis, Carnegie-Mellon University, 1996.

(41) Bominaar, E. L.; Block, R. *J. Chem. Phys.* **1991**, *95*, 6712.

(42) Babcock, G. T. In *Biological Aspects of Raman Spectroscopy*; Spiro, T. G., Ed.; Wiley: New York, 1988; pp 294−346.